VERIZONA PUBLISHER
Publishing Your Ideas

www.verizonaonlinepublishing.com

Vol: 2, Issue: 2

Journal of Nanoscience with Advanced Technology

Highly Sensitive Dual Quartz Reactance-to-Frequency Transducer

Vojko Matko* **and Miro Milanovic**

Faculty of Electrical Engineering and Computer Science, University of Maribor

***Corresponding author:** Vojko Matko, Faculty of Electrical Engineering and Computer Science, University of Maribor, Slovenia; Tel: +386-2-220-7111; E mail: vojko.matko@um.si

Article Type: Research, **Submission Date**: 21 February 2017, **Accepted Date:** 21 April 2017, **Published Date:** 03 August 2017.

Citation: Vojko Matko and Miro Milanovic (2017) Highly Sensitive Dual Quartz Reactance-to-Frequency Transducer. J Nanosci Adv Tech 2(2): 1-9. doi: https://doi.org/10.24218/jnat.2017.25.

Abstract

A new high sensitivity temperature-compensated reactance-to-frequency transducer with two quartz crystals oscillating in the switching oscillating circuit is presented. The novelty of this method lies in the switching-mode converter bringing a considerable reduction of the temperature influence of AT-cut crystal (the crystal's x axis is inclined by 35°15' from the z (optic) axis) frequency change in the temperature range between 10–50 °C and in the use of additionally connected sensing reactance in parallel to the shunt capacitances of the two quartzes. The oscillator switching method and parallel switching reactances connected to the quartz crystals do not only compensate crystals' natural temperature characteristics but also any other influences on the crystals such as ageing of both the crystals and other oscillating circuit elements. In addition, the method also improves reactance-to-frequency sensitivity, linearity and reduces the output frequency measurement error. The experimental results show that through high temperature compensation improvement of the quartz crystals' characteristics, this switching method theoretically enables a 100 zF resolution. It converts capacitance in the range 4–8 pF to frequency in the range 2–100 kHz.

Keywords: Dual quartz, Reactance-to-frequency transducer, Temperature compensation.

Introduction

The reactance-to-frequency conversion has become in recent years increasingly popular in a large variety of applications that are designed, for instance, for the measurement of a number of physical measurands, such as mechanical displacement, nanopositioning, eccentric motion, strain sensing [1-3], dielectric properties and density of liquids, small volumes or levels, pressure, flow, etc. Reactance-to-frequency conversion is also used in accelerometers, gyroscopes, and biosensors in medical and chemistry measurements. Typically, in many of them the reactance is first converted to the frequency signal and after that to physical or chemical quantity for analysis. Reactance-to-frequency conversion is also a well-established technique in microscale converters and represents a universal transduction mechanism for the measurements in which reactance changes need to be measured with great precision.

The idea for high resolution reactance-to-frequency transducer uses two quartz crystals with the switching oscillator circuit. Such use improves both reactance-to-frequency sensitivity and the linearity of the characteristics. It also compensates the temperature-frequency characteristics of two quartz crystals, enabling very stable transducer functioning in an extended temperature range. In addition, it also compensates the influence of any other electronic circuit element, and foresees the functioning of the sensitive capacitive element (in case reactances are capacitive) [4-7]. Temperature-wise, the new method makes possible a stable functioning of the small reactance conversion to a frequency signal with a small number of elements in a transducer.

Moreover, when compared also to some other methods [8-20] for the conversion of reactance to frequency, the newly proposed method also proved to have many advantages which include: compensation of quartz self-temperature characteristic, temperature compensation of all elements because of specific oscillator's circuit, compensated influence of the supply voltage on the oscillating circuit output signal, possibility to use of quartz crystals with different cutting angles [21,22], high circuit sensitivity and resolution. Another important factor of great importance is high dynamic stability during temperature changes in the extended operating range. The use of switching circuits in many instances improves electrical circuit characteristics and/or compensates certain influences [23-30].

Dual Quartz Crystal Impedance

The operation of a quartz crystal is frequently explained using the familiar "Equivalent Circuit", illustrated in Figure 1 (Q1 and

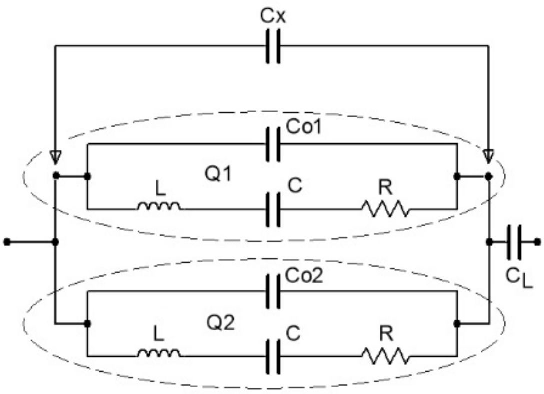

Figure 1: Two quartz crystal equivalent circuits connected in parallel

Q2) representing an electrical depiction of the quartz crystal unit [31-32].

In Figure 1, the capacitance labeled C_0 is a real capacitance, comprising the capacitance between the electrodes and the stray capacitance associated with the mounting structure. It is also known as the "shunt" or "static" capacitance, and represents the crystal in a non-operational, or static, state. The other components represent the crystal in an operational or motional state: *L*, *C*, and *R* identify the "motional inductance", the "motional capacitance", and the "motional resistance", respectively. The capacitance C_x is a parallel load capacitance.

The series resonance frequency f_s of the single quartz crystal is

$$f_s = \frac{1}{2\sqrt{LC}} \qquad (1)$$

The complex impedance equation for a single crystal equivalent circuit (Figure 1) is

$$\bar{Z} = \frac{\left(R + j\omega L + \frac{1}{j\omega C}\right)\cdot\frac{1}{j\omega C_0}}{R + j\omega L + \frac{1}{j\omega C} + \frac{1}{j\omega C_0}} \qquad (2)$$

If we define the frequency ratio $\Omega = \omega / \omega_0$, which depends on $\omega_0 = 1/\sqrt{L\cdot C}$, and taking into account $\omega_0 L = 1/\omega_0 C$, the impedance equation for a single crystal unit is [31]

$$\bar{Z}_q(\Omega) = R\frac{1 + j\frac{\omega_0\cdot L}{R}\left(\Omega - \frac{1}{\Omega}\right)}{1 + \frac{C_0}{C}\left(1-\Omega^2\right) + j\frac{C_0}{C}\cdot\frac{R}{\omega_0\cdot L}\cdot\Omega} \qquad (3)$$

The impedance equation for two quartz crystals connected in parallel can be written as a complex substitutional equation for both crystals

$$\bar{Z}_{qq}(\Omega) = \frac{\bar{Z}_q(\Omega)\cdot\bar{Z}_q(\Omega)}{\bar{Z}_q(\Omega) + \bar{Z}_q(\Omega)} \qquad (4)$$

As the capacitive load C_L in series with the crystal or capacitive load in parallel C_0 is varied, the crystal frequency is pulled (Figure 1). This change of the frequency with load capacitance is expressed by

$$f_L = f_S\cdot\sqrt{1 + \frac{C}{C_0 + C_L}} \approx f_S\left(1 + \frac{C}{2\left(C_0 + C_L\right)}\right) \qquad (5)$$

The frequency pulling range Δf_L (Equation 6) of the element is defined as the change in frequency produced by changing the load capacitance C_x from one value to another (Figure 1).

$$f_L = f_s\left(\sqrt{1 + \frac{C}{\left(C_0 + C_{x1}\right) + C_L}} - \sqrt{1 + \frac{C}{\left(C_0 + C_{x2}\right) + C_L}}\right) \qquad (6)$$

Since

$$\omega = \omega_0.\Omega = \frac{1}{2\sqrt{LC}}.\Omega \quad , \qquad (7)$$

the capacitive reactance for the capacitance C_x can be written as

$$\frac{1}{j_\omega C_x} = \frac{1}{j_{\omega 0}.\Omega C_x} \qquad (8)$$

The total impedance for the two crystals connected in parallel together with the capacitance C_x connected in parallel is expressed by

$$\bar{Z}_{qq}(\Omega) = \frac{\frac{\bar{Z}_q(\Omega).\bar{Z}_q(\Omega)}{\bar{Z}_q(\Omega) + \bar{Z}_q(\Omega)}\cdot\frac{1}{j\omega_0.\Omega.C_x}}{\left(\frac{\bar{Z}_q(\Omega).\bar{Z}_q(\Omega)}{\bar{Z}_q(\Omega) + \bar{Z}_q(\Omega)} + \frac{1}{j\omega_0.\Omega.C_x}\right)} \qquad (9)$$

Figure 2 shows that when two crystals are connected in parallel, the total complex part of impedance *Im* (*Zqq* (Ω)) is reduced, while the resonance frequency in relation to the change *Ω* remains at the frequency of 4 MHz approximately the same (Ω = 1.0011) compared to one single crystal. At frequencies of 10 and 19 MHz, the resonance frequency in relation to change *Ω* is higher (at $\Omega \cong 1.0022$) due to additional parasitic capacitance and inductance influences, however, compared to one single crystal it remains more or less the same. Reduced total reactance (due to connection in parallel) results in an easier crystal oscillation and pulling range increase by approximately 200% [6].

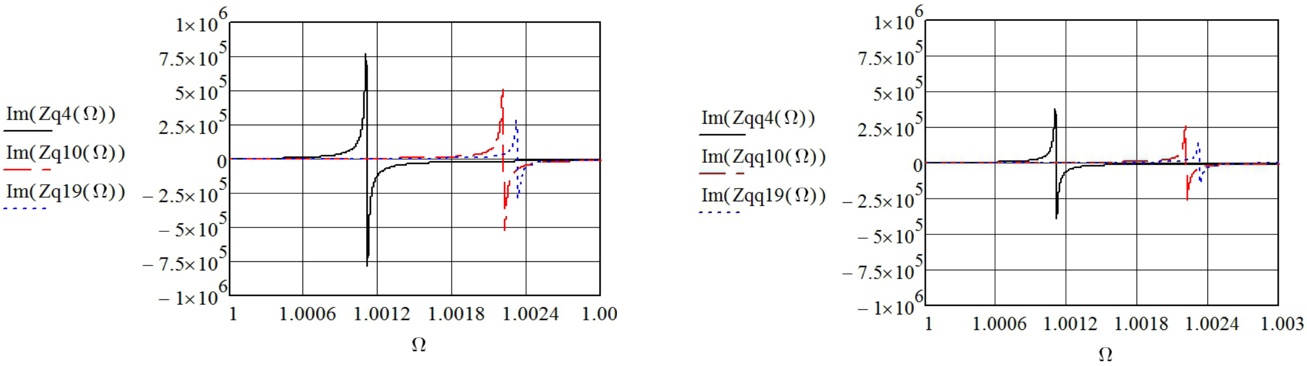

a b

Figure 2: Phase diagrams for **a)** a single- and **b)** dual-crystal unit operating at the oscillation frequencies of 4, 10 and 19 MHz

Reactance-to-Frequency Transducer Circuit

The proposed reactance-to-frequency transducer is based on an oscillator circuit with two quartz crystals and the switching part together (Figure 3). The novelty of the method described in this article lies in the use of specific symmetrical switching mode oscillator and additionally connected impedances Z_x and Z_{ref} in series with digital switch to the shunt capacitances C_{01} and C_{02} of the quartz crystals (Figure 1). The conversion impedance Z_x and reference impedance Z_{ref} are connected to the quartz crystal alternately in parallel and enable significant reduction of temperature influence on frequency change because of symmetry of the circuit. This yields high impedance-to-frequency sensitivity and simultaneous compensation of all other disturbing influences. The switching between the oscillator frequencies f_{o1} and f_{o2} is performed through the switching signal (*Sw, which can be 1 or 0*) and an additional circuit of NAND gate ((Negative-AND) is a logic gate which produces an output which is false only if all its inputs are true) (Figure 3). Inductance L_s is used for the simultaneous fine-tuning of the frequencies f_{o1} and f_{o2} and for the reactance $-j/\omega C_x$ to frequency sensitivity setting (in case the impedance Z_x is capacitive). The signal corresponding to the frequency difference between the frequency f_{o1} and reference frequency f_r or difference between the frequency f_{o2} and reference frequency f_r enters the LP (Low Pass) (which is a pulse wide modulated signal [33-35]). With the help of the reference frequency f_r, both signals f_{o1} and f_{o2} (4 MHz) are converted to the range between 2–100 kHz, which is suitable for the further signal processing. At the LP filter (with the response time of 2 μs) output, the triangular signal (with the initial setting frequency of 2 kHz depending on L_s and on Z_{ref}) is produced and then converted to a rectangular signal by Schmitt circuit representing the output signal. The output f_{out} thus represents the temperature and any other influence compensated frequency signal which is synchronously measured with regard to the switching frequency f_{Sw} = 10 Hz (thus the converter response time is 100 ms). Capacitance C_1 serves to suppress the spurious responses to avoid crystal oscillation at higher or lower frequencies [4].

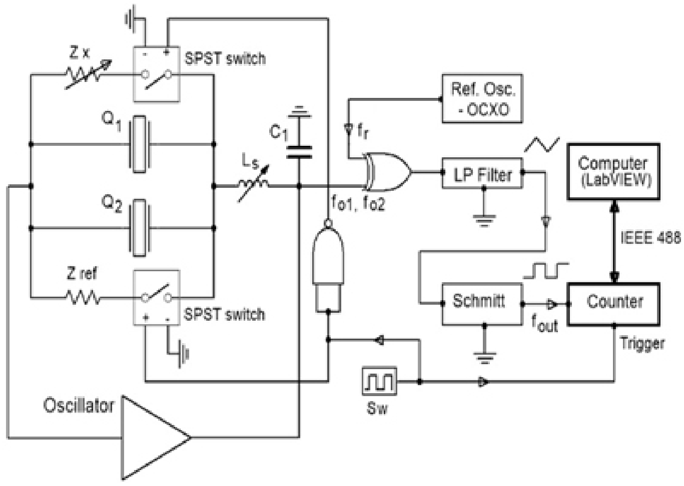

Figure 3: Schematic representation of the switching mode reactance-to-frequency transducer by analog SPST (Single-Pole Single-Throw) switch

A list of abbreviations:SPST switch – DG417 (analog switch); Ref. Osc. OCXO – OC18T5S (oven-controlled oscillator);

LP Filter – Low Pass filter; Schmitt – Schmitt hysteresis circuit; Sw – low frequency oscillator (0.2 – 5 Hz); Counter – programmable counter HM8122; Z_x– conversion impedance; Z_{ref}– reference impedance; Q_1, Q_2 – quartz crystals; L_s – inductance; C_1 – capacitor; C_x– parallel load changeable capacitor; C_{ref}– reference load capacitor; f_{o1} – oscillator frequency when SPST switch 1 is on; f_{o2} – oscillator frequency when SPST switch 2 is on; fr – reference frequency; fout – output frequency

When impedances Z_x and Z_{ref} are the same, f_{o1} and f_{o2} remain almost the same at states 1 and 0 of *Sw* signal Q $\bar{Q}$ Q and depend on the quartz crystal resonant frequency f_0, quartz crystals' temperature characteristics $\Delta f_0\,(T)$, its ageing $\Delta f_0\,(t)$, the L_s and Z_x and Z_{ref} inequality. $\Delta f(t)$ However, when the impedances Z_x and Z_{ref} are different, the frequencies f_{o1} and f_{o2} depend on the state of *Sw*, the quartz crystal series resonant frequency f_0, quartz crystal temperature characteristics $\Delta f_0\,(T)$, $\Delta f(T)$ its ageing $\Delta f_0\,(t)$, impedances $\Delta f_0\,(Z_x)$ and $\Delta f_0\,(Z_{ref})$, as well as Δf_0 (ΔL_s) $\Delta C_2\,\Delta L_2$ change $\Delta f(T)\,\Delta f(t)$ In case of the difference of the two frequencies f_{o1} and f_{o2} Q $\bar{Q}$, $\Delta f_0\,(T)$, $\Delta f_0\,(t)$, and Δf_0 (ΔL_s) are compensated because only one temperature quartz characteristics is involved.

The output frequency f_{out} depends on *Sw* signal, f_o and reference frequency f_r and can be expanded to (for $Sw = 1$ and for $Sw = 0$ in case $Z_x = 1/j\omega.C_x$ and $Z_{ref} = 1/j\omega.C_{ref}$):

$$f(Sw) - f_r = f_0 + \Delta f_0(T_1) + \Delta f_0(t_1) + \Delta f_0(L_s) + \Delta f_0(C_x) - (f_r(T_1) + \Delta f_r(T_1) + \Delta f_{cerr}(t_1) \tag{10}$$

$$f\left(\overline{Sw}\right) - f_r = f_0 + \Delta f_0(T_2) + \Delta f_0(t_2) + \Delta f_0(L_s) + \Delta f_0(C_{ref}) - (f_r(T_2) + \Delta f_r(T_2) + \Delta f_{cerr}(t_2) \tag{11}$$

where Δf_r (T) in (10) and (11) represents the temperature instability of the reference oscillator signal, and Δf_{cerr} (t) the counter error. The joining of f_0 and $\Delta f_0(C_x)$ gives (12) which represents f_{o1}. The particularity of this equation lies in the fact that it takes into account the compensation C_{01} and C_{02} (Figure 1) and at the same time linearizes the quartz characteristics due to the ΔC_x change (Figure 1) and allows for the sensitivity setting [6,7,22]

$$f(Sw,k,C_x) = \frac{1 + \dfrac{C}{2\left(\dfrac{1}{k}(C_{01} + C_{02} + C_x) - \dfrac{1}{\omega_0^{\,2}.k.L_s}\right)}}{2\pi.\sqrt{L.C}} + \Delta f_0(T_1) + \Delta f_0(t_1) \tag{12}$$

where:

k - sensitivity value (0.5, 1, 2),

ω_0 - quartz crystal series resonant frequency,

T - temperature,

t - time,

and ω_o is defined as (13)

$$\omega_0 = 2\pi f_0 \,. \tag{13}$$

The joining of f_0 and $\Delta f_0(C_{ref})$ gives (14) which represents f_{o2}.

$$f\left(\overline{Sw},k,C_{ref}\right) = \frac{1 + \dfrac{C}{2\left(\dfrac{1}{k}(C_{01} + C_{02} + C_{ref}) - \dfrac{1}{\omega_0^{\,2}.k.L_s}\right)}}{2\pi.\sqrt{L.C}} + \Delta f_0(T_2) + \Delta f_0(t_2) \tag{14}$$

Frequency sensitivity in (12) and (14) can be set with the value *k* [6], achieving at the same time simultaneous dependence linearization $\Delta f_0(C_{o1} + C_{o1} + \Delta C_x)$ [6,21,22,36]. At every switch between *Sw* signals, the frequency f_{out} is measured synchronously by the counter (Figure 3) [23] and its value is transferred to the LabVIEW software calculating the difference between the two frequencies. The switching between *Sw* signals Q also compensates the auxiliary frequency f_r, and consequently its frequency temperature instability as well. This gives the frequency difference in (15) representing the temperature-compensated value of the output frequency f_{out} depending almost uniquely on the difference between ΔC_x and ΔC_{ref} change.

$$\begin{aligned} \Delta f_{out}(C_x - C_{ref}) = {} & \left(f(Sw,k,C_x) - (f_r(T_1) + \Delta f_r(T_1)) + \Delta f_{cerr}(t_1)\right) - (\\ & -\left(\left(f\left(\overline{Sw},k,C_{ref}) - (f_r(T_2) + \Delta f_r(T_2)\right) + \Delta f_{cerr}(t_2)\right)\right) \end{aligned} \tag{15}$$

This means that $\Delta f_{out}(C_x\text{-}C_{ref})$ is independent of the quartz crystals' temperature characteristics $\Delta f_0(T)$, its ageing $\Delta f_0(t)$, frequency reference changes $\Delta f_r(T)$, circuit element temperature characteristics influences, but, on the other hand, dependent on the counter error Δf_{cerr} (t) in (15) and (16):

$$\Delta f_{out}(C_x - C_{ref}) = \frac{\dfrac{C}{2\left(\dfrac{1}{k}(C_{01} + C_{02} + C_x) - \dfrac{1}{\omega_0^{\,2}.k.L_s}\right)}}{2\pi.\sqrt{L.C}} + \Delta f_{cerr}(t_1) - \left(\frac{\dfrac{C}{2\left(\dfrac{1}{k}(C_{01} + C_{02} + C_{ref}) - \dfrac{1}{\omega_0^{\,2}.k.L_s}\right)}}{2\pi.\sqrt{L.C}} + \Delta f_{cerr}(t_2)\right) \tag{16}$$

The quartz stray capacitances C_{01} and C_{02} include the pin-to-pin input and output capacitances of the oscillator at the crystals' pins, plus any parasitic capacitances. The typical value of the stray capacitance is between 2.5 pF and 7 pF. This expands the possibility of the use of the frequency stable quartz crystal oscillator by influencing quartz crystal equivalent circuit as a capacitive transducer whose capacitance is in the range 4–8 pF. Stable oscillation and high sensitivity in this range [6,37-41] are thus one of this method's major advantages.

Frequency Stability of the Transducer

The frequency stability of the transducer such as wide operating temperature range, the use of various types of crystals and drive level should be considered because a stable oscillator circuit is of vital importance.

Generally, different temperature frequency curves are represented as cubical parabola with temperature inflection point at 25 °C, depending on the crystal cut angle and the mechanical construction. When using AT-cut crystals (cut angle: 0`) (The plate contains the crystal's x axis and is inclined by 35°15' from the z (optic) axis. The frequency-temperature curve is a sine-shaped curve with inflection point at around 25–35 °C) in oscillators, a frequency change in the oscillation up to few Hz of the crystal can be detected in the range between 10–50 °C [4,21]. The crystals used in the experiment (Figure 1) were AT-cut (cut angle: 0`) [8] crystals with the temperature change ±3 ppm in the range 0–50 °C. The data of the electrical quartz crystals' equivalent elements are f_0 = 4 MHz, *R* = 10 Ohm, *C* = 25 fF, *L* = 64 mH, C_o = 4 pF, quality *Q* = 80 k. The frequency f_0 was selected due to a greater oscillation amplitude and a higher *Q* value for the selected oscillation circuit. The new method (Figure 3) allows the AT-cut crystal temperature characteristics compensation (under 0.02 Hz) in the above temperature range through the switching circuit compensating this characteristics and reducing its influence to a minimum [22,37,42].

Stability of the electronic circuit depends upon the quartz crystal temperature stability and upon the circuit type and element quality (elements of the same values must be of the same quality). Oscillator frequency variation as a function of time is normally considered in short-term temperature stability (second-to-second) and long-term stability over years. The short-term stability of a quartz crystal depends on the actual oscillator design and is totally controlled by the quartz crystal at low drive levels (<20 μW) [4]. Long-term stability (ageing) is naturally greater during the first part of the crystal unit life (first year of operation). The ageing rates of the best cold weld crystals are less than ±1 ppm/year (0–50 °C) [5], [19,22]. The ageing of other electronic circuit elements is compensated in the same way. If the circuit supply voltage (5 V) (Figure 3) is changed for ±1 %, both frequencies f_{o1} and f_{o2} are changed for ±0.01 Hz, compensating the influence of the voltage change.

The switching method highly reduces the influence of the short- and long-term stability of the above described converter due to the compensation of the previously mentioned influences of the quartz crystals, the circuit as well as the influence of the difference method using additional reference frequency f_r. The reference frequency f_r is OCXO (oven-controlled oscillator) OCXO-OC18T5S [43] (4 MHz) with frequency stability ±0.01 ppm in temperature range 0°– +60 °C following the warm-up time of 2 min. Through *Sw* signals, the output frequency f_{out} compensates all influences, including those of the reference frequency f_r. It is measured by the HM8122 counter (with the accuracy of $\pm 5\times10^{-9}$ (through the entire working temperature range from 0–50 °C)) [23]. The counter measurement error is then minimised by the LabVIEW software by subtraction of the two frequencies depending on *Sw* signals.

Experimental Results and Discussion

For this experiment, a prototype electronic circuit was produced guaranteeing physically stable conditions at the capacitance C_x, C_{ref} settings and inductance L_s (Figure 3). Stable parasite capacitances and inductances assure repeatability of the experimental results.

Figure 4 shows oscillator's frequency characteristics f_o with regard to the change of the capacitance C_x and a comparison of the characteristics for various sensitivity values L_s = (25 μH, 50 μH, 73 μH) and for state of *Sw* = 1 (T = 25 °C). The inductance L_s = 73 μH (2Q – two quartz crystals in parallel) records the highest sensitivity, i.e. 24 kHz/pF in the range 4–8 pF. The results show linearity of 0.1% of the capacitance-frequency characteristics (2Q – 73 μH) in the range 4–8 pF. The settings of C_x is in steps of 1pF with laser trim capacitors which have tolerance of 0.1% [44]. However, for this particular experiment, the capacitors C_x and inductance L_s with tolerance of 0.1% were specially selected [45-48] by the measurement with HP 4194A impedance/gain phase analyzer.

Figure 5 shows capacitance-frequency characteristics f_{out} (*Sw*) of the converter with regard to the change of the capacitance C_x from 4–8 pF (linear dependency $f_o(C_x)$ for 2Q (Figure 4)) and a comparison of the characteristics for a single quartz crystal and two quartz crystals for sensitivity value L_1 = 73 μH (Figure 4) and for the state of *Sw* = 1. For two quartz crystals, the linearity and sensitivity is better than for a single one in the range 4–8 pF (Figure 4). The linearity with two quartz crystals is improved by *k* value as shown in (12) and (14). The switching method compensates the temperature influence of the quartz crystal and oscillator circuit elements, and also compensates aging of all oscillator circuit elements as shown in (15) and (16). With the help of the reference frequency f_r, both signals f_{o1} and f_{o2} (4 MHz) are converted to the range between 2–100 kHz. If capacitances C_x and C_{ref} (Figure 3) are the same, f_{out} = 2 kHz (for both *Sw* signals), which means that f_r is by 2 kHz higher than f_{o1} and f_{o2} (initial settings by f_r).

Figure 6 shows a typical frequency f_{out} variation occurring when the transducer does not function as a switching mode transducer. The frequency f_{out} in such a case stands for the difference of frequencies f_{out} (*Sw*) = (f_o - f_r) where the output frequency changes depend on the temperature changes and the changes of the logical *Sw* signal condition, which can either have the value of 1 or 0. The frequency difference in this experiment

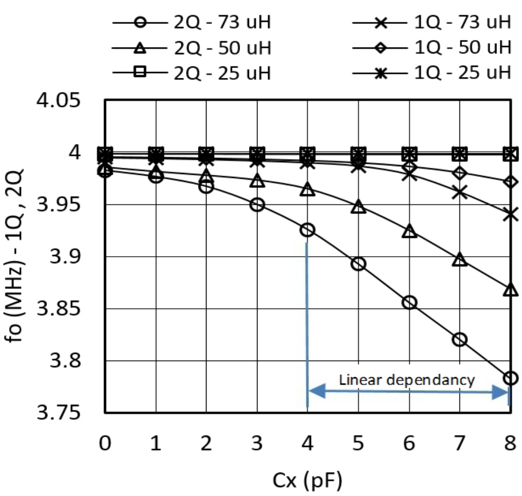

Figure 4: Capacitance-frequency characteristics f_o (for different sensitivities determined by inductance L_s for a single quartz crystal and two quartz crystals in parallel)

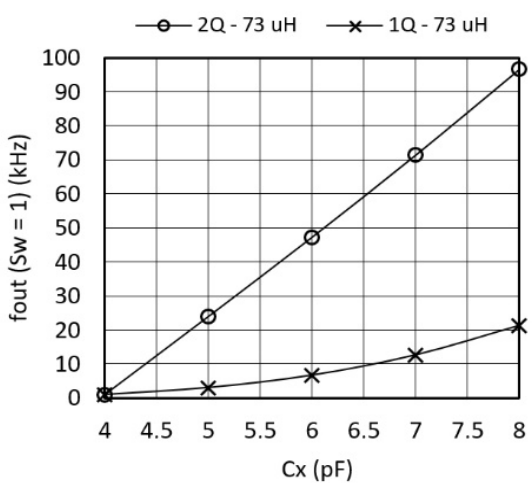

Figure 5: Capacitance-frequency characteristics of the converter for a single quartz crystal and two quartz crystals in parallel and sensitivity setting for both by inductance L_s = 73 μH

is set by the reference frequency f_r to approximately 2 kHz as shown in Figure 6. The dotted line marks the frequency increase within the temperature range T = 25 °C ± 1 °C. Otherwise, the variation of the frequency f_{out} (t) for both conditions of the *Sw* signal is roughly the same. The switching mode method, on the other hand, was introduced to compensate for the changing of f_{out} resulting from the temperature changes. The idea behind is to have a capacitive frequency transducer with as high temperature stability and measurement resolution as possible. A comparison to the method using OCXO oscillators reveals that these have a greater stability in the range of 0.01 ppm, however, as they are hermetically closed, open access to the crystal which is required for the suggested method is not possible.

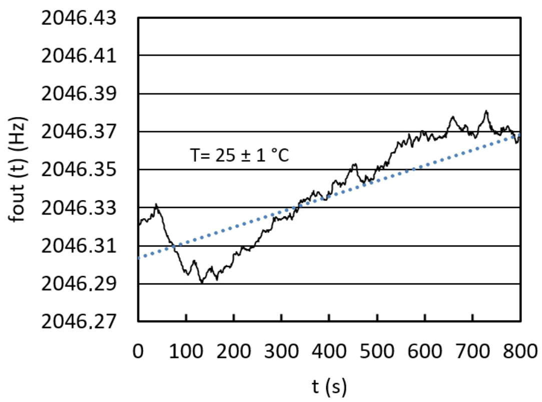

Figure 6: The frequency f_{out} (t) variation occurring when the transducer does not function as a switching mode transducer

Generally, two oven controller techniques are in common use for the purpose of maintaining a constant temperature on the crystal assembly. They are the switching controller and the proportional controller. The switching controller turns the power off when the maximum temperature is reached and on at the minimum level much like a home thermostat. The proportional oven controller varies the current to the heather or the duty cycle of the heather voltage inversely based upon the offset of the oven temperature from the desired level [43]. The OCXO oscillator crystals have a different angle of cutting (SC-cut), a different temperature characteristics and a turnover point at 85 °C.

Figure 7 experimentally shows the switching mode extended dynamic stability – the frequency change of f_{out} (*Sw*) (which in this experiment differs by 0.3 Hz) if the converter is influenced by a temperature changing from T_1 = 24 °C to T_2 = 26 °C. Figure 7 also demonstrates that the temperature influence on f_o and reference frequency f_r (in the time span between 0–300 s) changes the frequency difference (f_{o1} - f_r) and (f_{o2} - f_r) representing f_{out} in the same size class, which is why the f_o and f_r influence is compensated. Similarly, the frequency measurement error influence produced by the frequency counter (Figure 3) is significantly reduced. The dynamic change of both frequencies is approximately the same. The frequency shift between (f_{o1} - f_r) and (f_{o2} - f_r) depends on the difference between C_x and C_{ref}.

Figure 8 shows the short-term temperature-frequency stability (during the temperature shock produced by a hairdryer) for the frequency differences f_{out} (*Sw*) = (f_{o1} - f_r) and f_{out} = (f_{o2} - f_r) (at the beginning of the temperature shock the stable frequencies were 447 Hz and 504 Hz) occurring when the temperature in the range between 10 °C and 50 °C at the state *Sw* and and the determined sensitivity by value *L* = 73 μH (Figure 3) is changed. The A range (Figure 8) represents the frequency changes occurring during the instant temperature change from 10–50 °C. The B range, on the other hand, illustrates slower frequency changes (f_{o1} - f_r) and (f_{o2} - f_r) during the cooling back to 10 °C.

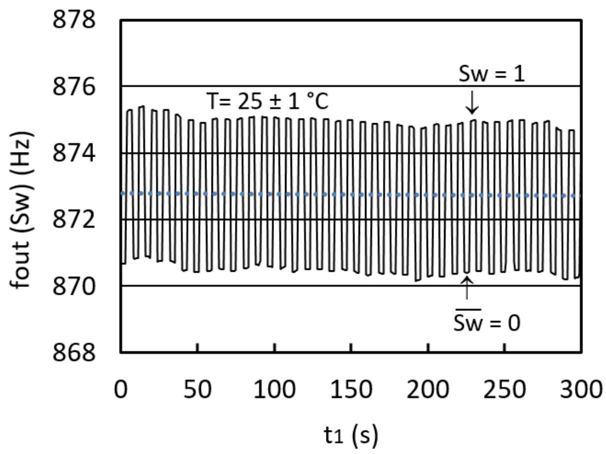

Figure 7: Extended temperature dynamic frequency stability for f_{out}(Sw=1) = (f_{o1} - f_r) and f_{out}(Sw=0) = (f_{o2} - f_r)

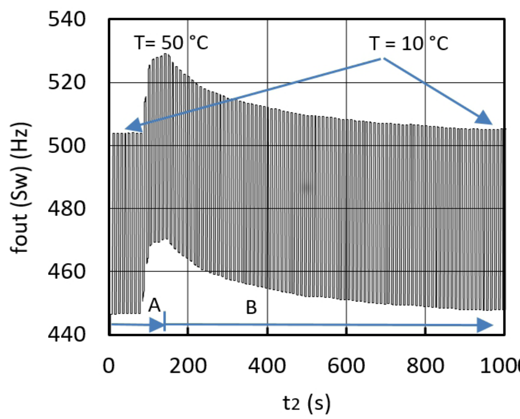

Figure 8: Short-term frequency stability (f_{o1} - f_r) and (f_{o2} - f_r) occurring when changing the temperature in the range 10–50 °C (measurement time: 1000 s)

Figure 9 illustrates frequency stability for Δf_{out} (*Sw*) at frequency difference 57 Hz between (f_{o1} - f_r) and (f_{o2} - f_r) during the temperature change (Figure 8) in the range 10–50 °C determined by the fixed C_x and C_{ref} once both frequencies are deducted (f_{o1} – (f_r + Δf_r)) – (f_{o2} – (f_r + Δf_r)). Deduction of both frequencies in relation to *Sw* signals is performed by LabVIEW software. In addition, Figure 9 also illustrates the temperature compensation of the quartz crystal natural temperature characteristics.

The comparison of results in Figure 8 and Figure 9 shows that the dynamic temperature influence (Figure 8) on the frequency change (f_{o1} - f_r) and (f_{o2} - f_r) in relation to *Sw* signal is approximately the same and well dynamically compensated at the output of the transducer as illustrated by Figure 9. The latter also shows high frequency dynamic stability (Figure 9) (C) in the range ±0.002 Hz), in which the environment temperature does not change so quickly anymore (Figure 8). If the change of the output frequency sensitivity f_{out} = 24 kHz/pF (Figure 5 2Q-73 μH) is in the temperature range between 10−50 °C and the supply voltage stability is 5 V ±0.01 V, the frequency reference f_r stability 0.01 ppm, then frequency stability at the output f_{out} = ±0.002 Hz, which gives the converter resolution ±100 zF.

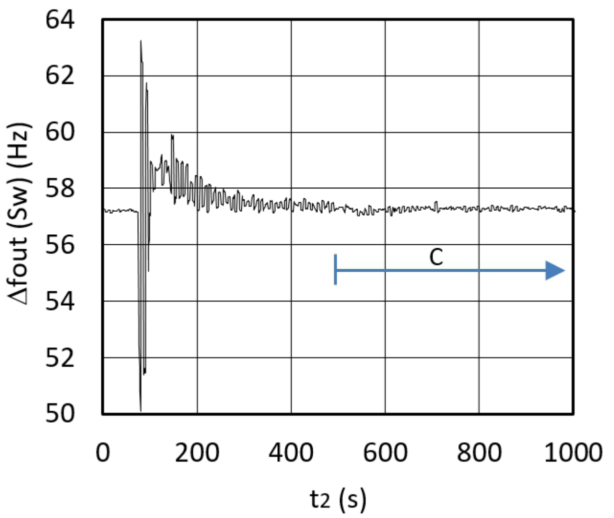

Figure 9: Output frequency dynamic error $\Delta f_{out} = (f_{o1} - (f_r + \Delta f_r)) - (f_{o2} - (f_r + \Delta f_r))$ during the change of temperature from 10 °C to 50 °C and back to 10 °C (measurement time: 1000 s)

Experimental circuit (Figure 10) is divided into two parts, where the left part is a switching section for C_x, C_{ref} and L_s settings by dip switches. This design was used to achieve as stable parasitic capacitances and inductances in the circuits as possible. The right part is intended for the oscillator switch time settings and an appropriate switching logic. Temperature measurements were performed near both crystals in the middle of the experimental circuit to detect short-term temperature changes. Figure 10 (right side) also shows additional oscillator, the trimmer for the switch time settings, and the connection part to the computer. Every single time, the oscillator's positive front triggers the measurement of the counter frequency. In this way, the frequency counter works synchronously with the *Sw* signal. The counter measures the frequency f_{out} one or more times at the *Sw* logical conditions 1 or 0. In addition, LabView software driver also makes possible within one *Sw* condition a statistical evaluation of a number of performed consecutive measurements. The left side (Figure 10), on the other hand, contains a room temperature measuring device measuring the temperature in the close vicinity of the quartz crystals and the experimental circuit. Its measuring probe is actually situated in the centre of the circuit. This position is particularly important for the measurement of the dynamical stability of switching mode reactance-to-frequency transducer during the temperature shocks produced by a hairdryer or uncontrolled temperature changing of the experimental circuit.

For this experiment, reactance-to-frequency converter was experimentally produced in the SMD technology on Al_2O_3 ceramics (Figure 10). At the front side of the housing, the converter has the pins for C_x, C_{ref} (Z_x, Z_{ref}) and at the back side of the housing, it has pins for supply voltage 5V, *Sw* signal and output frequency f_{out}. Capacitances C_x and C_{ref} can be directly connected to the pins as shown in the final design of the converter. From the practical point of view, parasitic capacitances otherwise added by the cables are reduced. For specific industrial purposes, capacitance C_{ref} can also be placed inside the housing. The main advantage of such a construction is that it allows the connection of the capacitance sensitive elements to these pins without any additional wires with additional parasitic capacitances. Connections made in this way introduce minimal parasitic capacitances, and even these are –when using switching method – reduced to minimum.

Conclusion

The experimental results show that the switching method excellently compensates quartz crystal non-linear frequency-

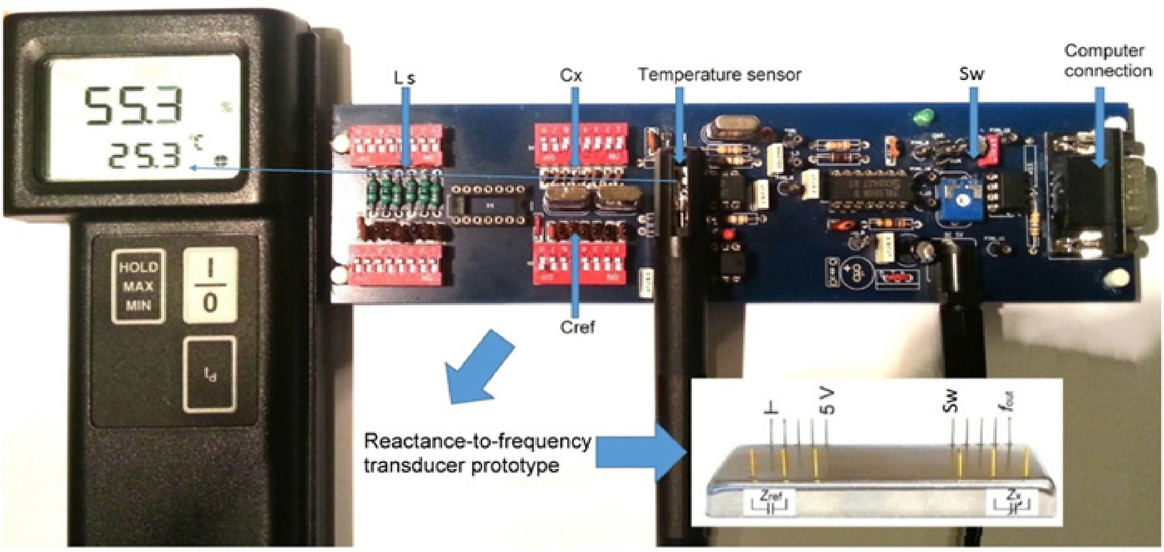

Figure 10: Experimental circuit and final reactance-to-frequency transducer design with connection pins for industrial use

temperature characteristics, its ageing and oscillator circuit elements, the influence of the supply voltage on the oscillating circuit, as well as the reference frequency f_r temperature instability and reduces counter error. The great advantage of the proposed method is that it resolves the issue of high sensitivity, linearity and at the same time the temperature compensation of the crystal characteristics and those of other elements, as well as the frequency stability after temperature compensation. The experimental results shown in the article relate to a significantly wider frequency range (2-100 kHz) with zeptoFarad resolution than is usually covered by practical measurements. The reference frequency f_r instability and the frequency counter measurement error is also greatly reduced.

The results clearly show that the oscillator switching method for high-precision reactance-to-frequency transducing opens up new possibilities through the self-temperature compensation of the main oscillating element and other disturbing influences. This makes this switching method a very interesting tool for the reactance-to-frequency converter especially because of the zeptoFarad resolution which is highly promising in various fields of physics, chemistry, mechatronics, biosensor technology and in specific high-quality production industries.

References

1. KentonBJ, LeangKK. Design and control of a three-axis serial-kinematic high-bandwidth nanopositioner.IEEE/ASME Trans. Mechatronics.2012; 17(2):356-369.
2. ChengMH, Chiu GTC, FranchekMA. Real-time measurement of eccentric motion with low-cost capacitive sensor. IEEE/ASME Trans.Mechatronics. 2013; 18(3):990-997.
3. Laflamme S, SaleemHS, Vasan BK, Geiger RL. Soft elastomeric capacitor network for strain sensing over large surfaces.IEEE/ASME Trans. Mechatronics.2013; 18(6):1647-1654.
4. Walls FL,Vig JR. Fundamental limits on the frequency stabilities of crystal oscillators.IEEE Trans. Ultrason. Ferroelectr. Freq. Control. 1995;42:576-589.
5. Filler RL,VigJR. Long-term aging of the oscillators.IEEE Trans. Ultrason. Ferroelect. Freq. Cont. 1992; 39:241-249.
6. Matko V, JezernikK.Greatly improved small inductance measurement using quartz crystal parasitic capacitance compensation. Sensor. 2010; 10:3954-3960.
7. BandeyHL, MartinSJ, CernosekRW, HillmanAR.Modelling the responses of thickness-shear mode resonators under various loading conditions.Anal. Chem. 1999; 71:2205-2214.
8. ArnauA. A review of interface electronic systems for AT-cut quartz crystal microbalance applications in liquids. Sensors. 2008; 8:370-411.
9. Kurosawa S, TawaraE.Oscillating frequency of piezoelectric quartz crystal in solutions.AnalyticaChimicaActa. 1990; 230:41-49.
10. Davis KA, Leary TR. Continuous liquid-phase piezoelectric biosensor for kinetic immunoassays. Anal. Chem. 1989; 61:1227-1230.
11. Behling C, Lucklum R, HauptmannP.Possibilities and limitations in quantitative determination of polymer shear parameters by TSM resonators. Sensors and Actuators A. 1997; 61:260-266.
12. CamesanoTA, LiuYT, DattaM. Measuring bacterial adhesion at environmental interfaces with single-cell and single-molecule techniques. Advances in Water Resources. 2007; 30:1470-1491.
13. HugTS. Biophysical methods for monitoring cell-substrate interactions in drug discovery. Assay and Drug Development Technologies. 2003; 1:479-488.
14. DickertFL, Lieberzeit P, HaydenO. Sensor strategies for micro-organism detection – from physical principles to imprinting procedures. Analytical and Bioanalytical Chemistry. 2003; 377:540-549.
15. Bizet K, Grabielli C, PerrotH. Biosensors based on piezoelectric converters. Analysis EurJAC. 1999; 27:609-616.
16. Ni R, Zhang XB, Liu W, Shen GL, YuRQ. Piezoelectric quartz crystal sensor array with optimized oscillator circuit for analysis of organic vapours mixtures. Sensors and Actuators B. 2003; 88:198-204.
17. Rodriguez-Pardo L, Farina J, Gabrielli C, Perrot H, BrendelR. Resolution in quartz oscillator circuits for high sensitivity microbalance sensors in damping media. Sensors and Actuators B. 2004; 103:318-324.
18. Rodriguez-Pardo L, Farina J, Gabrielli C, Perrot H, BrendelR. Quartz crystal oscillator circuit for high resolution microgravimetric sensors. Electronics Letters. 2006; 42:1065-1067.
19. Ferrari V, Marioli D, TaroniA. Improving the accuracy and operating range of quartz microbalance sensors by purposely designed oscillator circuit. IEEE Trans. Instrum. Meas. 2001; 50:1119-1122.
20. Ferrari M, Ferrari V, Marioli D, Taroni A, Suman M, DalcanaleE. In-liquid sensing of chemical compounds by QCM sensors coupled with high-accuracy ACC oscillator. IEEE Trans. Instrum. Meas. 2006; 55:828-834.
21. GagnepainJJ. Sensitivity of quartz oscillator to the environment: Characterization methods and pitfalls.IEEE Trans. Ultrason. Ferroelect. Freq. Cont. 1990; 37:347-354.
22. Stanford Research Systems. [cited 2014 Jun] QCM100- Quartz crystal microbalance theory and calibration. [Online]. Availableat:http://www.thinksrs.com/downloads/PDFs/ApplicationNotes/QCMTheoryapp.pdf
23. Model HM8122 counter, Hameg Instruments (Germany).
24. Taib N, Metidji B, Rekioua T, FrancoisB. Novel Low-Cost Self-Powered Supply Solution of Bidirectional Switch Gate Driver for Matrix Converters . IEEE Trans. on Industrial Electronics. 2012; 59(1):211-219.
25. DriscollMM. Oscillator AM-to-FM Noise conversion due to the dynamic frequency-drive sensitivity of the crystal resonator. IEEE FCS. 2008:672-676.
26. Rohde UL,Poddar AK. Mode-Coupling and Phase-Injection mechanism enables EMI-Insensitive crystal oscillator circuits. IEEE TELSIKS. 2009:21-28.
27. Laurin JJ, Zaky SG, Balmain KG.EMI-Induced failures in crystal oscillators. IEEE Trans. on Electromagnetic Compatibility. 1991; 33(4):334-342.
28. YuenKY, Fleming A, MoheimaniS. A novel piezoelectric strain sensor for simultaneous damping and tracking control of a high-speed nanopositioner.IEEE/ASME Trans. Mechatronics. 2013; 18(3):1113-1121.
29. Mercedes E, Zhang J, Tan X, SepulvedaN. Roust control of VO2-coated microbenders using self-sensing feedback. IEEE/ASME Trans. Mechatronics. 2014; 19(5):1583-1592.

30. Qin Y, Tian Y, Zhang D, Shirinzadeh B, FatikowS. A novel direct inverse modelling approach for hysteresis compensation of piezoelectric actuator in feedforward applications.IEEE/ASME Trans. Mechatronics. 2013; 18(3):981-989.
31. Schrüfer E. Electrical Measurement: Quartz as a Frequency reference. München, Wien: Carl Hanser Verlag; 1992. p. 405- 412.
32. Meeker TR. Theory and Properties of Piezoelectric Resonators and Waves: In Precision Frequency Control. Academic Press. 1985; 1:47-119.
33. Chia-AnYeh,Yen-Shin Lai. Digital Pulsewidth Modulation Technique for a Synchronous Buck Converter to Reduce Switching Frequency. IEEE Trans. on Industrial Electronics. 2012; 59(1):550-561.
34. Zhao Z, Lai JS, ChoY. Dual-Mode Double-Carrier-Based Sinusoidal Pulse Width Modulation Inverter With Adaptive Smooth Transition Control Between Modes.IEEE Trans. on Industrial Electronics. 2013; 60(5):2094-2103.
35. KiatsookkanatornP, SangwongwanichS. A Unified PWM Method for Matrix Converters and Its Carrier-Based Realization Using Dipolar Modulation Technique. IEEE Trans. on Industrial Electronics. 2012; 59(1):80-92.
36. Wang S, LeeF. Analysis and applications of parasitic capacitance cancellation techniques for EMI suppression. IEEE Trans. Ind. Electron. 2010; 57(9):3109-3117.
37. Brice JC. Crystals for quartz resonators. Reviews of Modern Physics. 1985; 57:105-138.
38. MeekerTR. Theory and properties of piezoelectric resonators and waves.Precision Frequency Control, Academic Press. 1985; 1:47-119.
39. Miller LG, Wagner ER. Resonant phase shift technique for the measurement of small changes in grounded capacitors.Rev. Science Instrumentation. 1990; 61:1267.
40. Kao P, Allara D, TadigadapaS.Fabrication and performance characteristics of high-frequency micromachined bulk acoustic wave quartz resonator arrays.Meas. Sci. Technol.2009.doi: 10.1088/0957-0233/20/12/124007.
41. Marioli D,SardiniE.Measurement of small capacitance variations. IEEE Trans. Instrum. Meas. 1991; 40(2):426-428.
42. Wu IC, Lo CW, Fong KL. Method and apparatus for a crystal oscillator to achieve fast start-up time, low power and frequency calibration.United States patent US Patent No 7, 348, 861 B1. 2008 Mar 1.
43. Euroquartz. OCXO OC18T5S, Frequency reference. [Online]. Availableat: http://www.euroquartz.co.uk/Portals/0/oc18t5s.pdf
44. Johnson Technology. JMC. [cited 2014 Jun] [Online]. Availableat: http://www.johansontechnology.com.
45. Vijay K, Vinoy KJ, JoseKA.MEMS Inductors and capacitors, RF MEMS and their applications.NY: John Wiley & Sons; 2003. p. 183-240.
46. Yamaguchi M, Mastumo M, Ohzeki H, Arai KI. Fabrication and basic characteristics of dry-etched micro inductors. IEEE Trans. Magnet. 1990; 26:2014-2016.
47. GreenhouseHM. Design of planar rectangular microelectronic inductors.IEEE Trans. Parts Hybrids Packag. 1974; 10:101-109.
48. Yamaguchi M, Mastumo M, Ohzeki H,Arai KI. Analysis of the inductance and the stray capacitance of the dry-etched micro inductors. IEEE Trans. Magnet. 1991; 27:5274-5275.